NJC

ROYAL SOCIETY OF CHEMISTRY

PAPER

View Article Online
View Journal | View Issue

Cite this: *New J. Chem.*, 2025, **49**, 10205

Complexation driven synthesis of nickel ferrocyanide nanoparticles for non-enzymatic glucose sensing application using field effect transistors and microcontroller-based platforms†

Chandan Saha,[a] Pooja Kumari,[a] Sarit K Ghosh,[a] Harishchandra Singh[b] and Kaushik Mallick *[a]

The new generation of glucose biosensors has gained attention for their rapid response, stability, reproducibility and low detection limit. Their affordability and high sensitivity make them ideal for both clinical and non-clinical applications. This study explores the synthesis of nickel ferrocyanide (NFC) using a complexation-mediated route and investigates its potential application as a glucose sensor. Structural and compositional analysis (X-ray diffraction, transmission and scanning electron microscopy, X-ray photoelectron spectroscopy and Raman spectroscopy) confirmed the formation of NFC nanoparticles. Electrochemical studies revealed strong catalytic activity of the synthesized material toward glucose oxidation, driven by Ni(II)/Ni(III) redox transitions, in alkaline media. To translate these functionalities into a practical sensing platform, an extended-gate field-effect transistor (EG-FET) setup was developed, allowing for selective and stable glucose detection. Additionally, a microcontroller-based system was developed for real-time signal acquisition and wireless data transmission, enabling a portable and user-friendly glucose monitoring solution. The EG-FET and microcontroller based sensors present a scalable and efficient approach for glucose sensing, demonstrating significant potential for biomedical applications.

Received 26th February 2025,
Accepted 15th May 2025

DOI: 10.1039/d5nj00874c

rsc.li/njc

1. Introduction

Glucose is a carbohydrate-based biomolecule, specifically a monosaccharide, and serves as the primary source of adenosine triphosphate, which provides energy to cells throughout the body.[1] Abnormal glucose levels can cause various physiological and behavioural issues.[2] An increase of glucose levels in human physiological fluids causes a chronic metabolic disorder called diabetes mellitus, considered one of the most prevalent diseases.[3,4] Thus, the regular monitoring of glucose in the body is required to prevent the progression of diabetes. Several analytical methods have been reported in the literature for the determination of physiological glucose concentration.[5–10] Among the various conventional analytical methods, electrochemical sensors offer rapid solutions due to fast response speed, high sensitivity and selectivity creating an intriguing and promising class of analytical tools.[11]

The electrochemical method primarily employs two specific techniques, namely potentiometric and amperometric methods, for monitoring glucose concentrations. In the potentiometric method, the potential difference between the reference electrode and the working electrode is measured at zero applied current. It is generally used to measure glucose concentration in the order of micro-molar levels, allowing for selective and sensitive detection.[12,13] In the amperometric method the current is measured under constant potential. During the chemical reaction of glucose, electrons are generated, causing the current to flow. The magnitude of the resulting current is dependent on the glucose concentration.[14] Recently, there has been increasing interest in biosensors that utilize field-effect transistors, primarily because of their significant advantages, such as the ability to amplify current and achieve a high signal-to-noise ratio. This makes an effective system for detecting low concentrations of biomolecules, as the enhanced signal quality allows for more precise and reliable measurements. As a result, field-effect transistor based biosensors are gaining attention for practical use.[15]

Two major types of electrochemical glucose biosensors that have been widely studied are enzymatic and non-enzymatic glucose biosensors.[16–18] While enzymatic glucose sensors offer high sensitivity, they are prone to limitations caused by external

[a] *Department of Chemical Sciences, University of Johannesburg, P. O. Box: 524, Auckland Park, 2006, South Africa. E-mail: kaushikm@uj.ac.za*
[b] *Nano and Molecular Systems Research Unit, University of Oulu, FIN-90014, Finland*

† Electronic supplementary information (ESI) available. See DOI: https://doi.org/10.1039/d5nj00874c

factors like humidity, pH, and temperature fluctuations.[19] To overcome these issues, significant focus has been placed on developing non-enzymatic glucose sensors. A variety of materials have been explored for enzyme-free glucose sensors, including precious metals, metal oxide nanoparticles, organic–inorganic hybrid systems and carbon-based materials.[18,20–24] Among the various inorganic materials, nickel-based systems are an excellent choice for glucose sensors due to their conductivity, natural abundance, biocompatibility and multi-valency properties.[1,25] The above characteristics of nickel-based systems are believed to improve the catalytic activity for glucose oxidation owing to the formation of a Ni^{2+}/Ni^{3+} redox couple in an alkaline medium.[1]

In line with our ongoing research aimed at developing effective catalyst systems for various sensing applications,[18,26–28] we have found, in this work, that aniline-immobilized nickel ferrocyanide, prepared through a complexation-mediated route, serves as an efficient material for glucose sensing application. Cyclic voltammetry techniques were employed to investigate glucose-catalyst interactions, while an extended-gate field-effect transistor based sensor was used as an emerging detection approach. Additionally, a micro-controller based potentiometric sensing system was developed for remote glucose monitoring and enabling real-time data transmission to an online platform.

2. Experimental

2.1. Materials

Analytical grade aniline, nickel chloride, potassium ferrocyanide, glucose, acetaminophen, lactate, fructose, cholesterol and sucrose. Were purchased from Merck and used directly in this study without further purification. Indium tin oxide coated polyethylene terephthalate films (ITO-PET) and Fusayama/Meyer Artificial Saliva solution were received from Sigma Aldrich.

2.2. Synthesis of aniline stabilized nickel ferrocyanide (NFC) nanoparticles

To synthesize NFC, 3 mL of aniline was first dissolved in 10 mL of methanol. Then, 7 mL of a 0.1 M aqueous potassium ferrocyanide solution was added, leading to the formation of a white precipitate, which was identified as a ferrocyanide–aniline complex. The resulting precipitation was then subjected to the dropwise addition of 5 mL of a 0.1 M nickel chloride solution while stirring. This process led to the formation of NFC, which exhibited a celadon green color. The solid product was isolated by filtration, and then dried under vacuum at 60 °C. It was subsequently characterized using various analytical techniques to confirm its structure and properties. The synthesized NFC was then employed as a catalyst for glucose sensing applications.

2.3. Material characterization

The synthesized material was thoroughly characterized using multiple analytical techniques. X-ray diffraction (XRD) was conducted with a PANalytical X'pert diffractometer, while morphological analysis was performed using transmission electron microscopy (TEM, JEOL JEM-2100). Surface chemistry was examined through X-ray photoelectron spectroscopy (XPS) using a Thermo Scientific MultiLab 2000. Raman spectra were measured using a Jobin-Yvon T64000 Raman spectrometer. Electrochemical and potentiometric analyses were carried out using a Bio-Logic SP-300 and an Arduino Uno R4 Wi-Fi, respectively.

2.3.1. Electrochemical cell assembly. A three-electrode system comprising a glassy carbon electrode (GCE), an Ag/AgCl electrode and a platinum wire as the working, reference and counter electrodes, respectively, was immersed in an electrochemical cell containing 6 mL of NaOH solution (10 mM). The GCE was polished with 0.05 μm alumina, rinsed with alcohol and dried under a heating lamp. The catalyst was deposited onto the working electrode using the following procedure. In a typical preparation, 1.0 mg of NFC, $Ni_2[Fe(CN)_6]$, was dispersed in a mixture of 100 μL methanol and 10 μL Nafion. A 10 μL aliquot of this dispersion was then drop-cast onto the polished electrode and allowed to dry under a heating lamp.

2.3.2. Fabrication of the NFC coated ITO electrode. A 30 μL slurry containing NFC was spin-coated onto an indium tin oxide-coated polyethylene terephthalate (ITO-PET) substrate (1 cm × 2 cm, with a surface resistivity of 60 Ω) at 1800 rpm for 180 seconds. The process was repeated three times to ensure uniform film formation, followed by drying at 80 °C in a hot air oven to improve film adhesion.

2.4. Circuit diagram for the EG-FET sensor

Fig. 1A represents the circuit diagram of the extended-gate field-effect transistor (EG-FET). The commercially available integrated circuit (CD4007UB) was used as the key component of the sensor. The source and drain of the n-type MOSFET were connected to a Keithley 2614B (SMU 2) source meter, while the gate electrode received voltage from SMU 1 *via* the reference and extended gate electrode (EGE).

2.5. Circuit diagram for the arduino-based sensor

A microcontroller-based glucose sensor was developed as illustrated in Fig. 1B. The setup consisted of a working and a reference electrode immersed in NaOH (10 mM). The working electrode was grounded, while the reference electrode was connected to the analog pin A0 of the microcontroller (Arduino Uno). A 1602 I2C LCD module, powered by 5 V supply, was interfaced *via* the SDA and SCL lines, linked to analog pins A4 and A5, respectively. The R4 version of the Arduino Uno, equipped with a 12-bit ADC and a reference voltage of 3.3 V, achieved a resolution of approximately 0.8 mV per bit. The voltage measurements are displayed on the LCD and visualized using Python Matplotlib.

2.6. Internet of things (IoT) implementation

IoT integration was enabled using the onboard ESP32 module of the Arduino Uno R4. The processed data were transmitted to the ThingSpeak cloud platform (MathWorks, USA) for remote

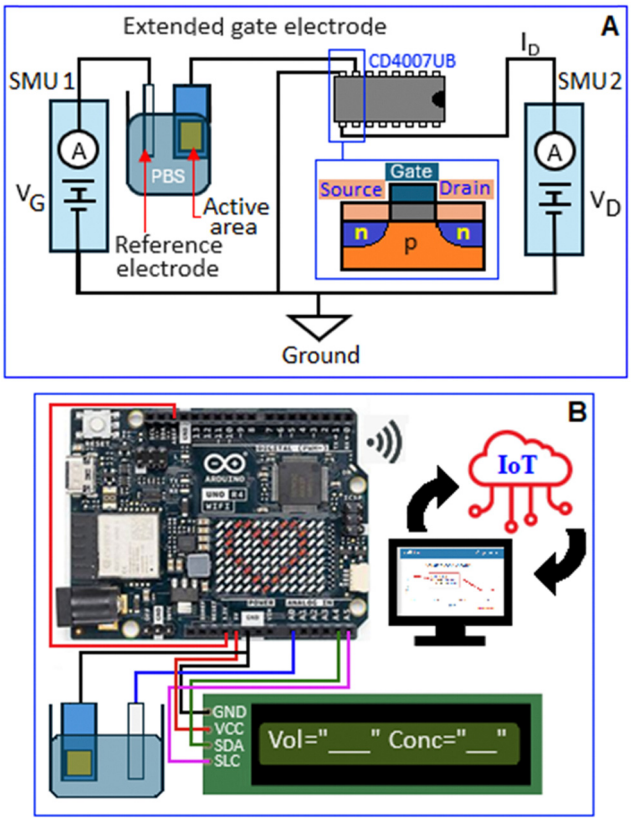

Fig. 1 Circuit diagram of (A) EG-FET based and (B) microcontroller (Arduino Uno) based glucose sensor.

access. The Wi-Fi connectivity was established through the program defined in the Arduino IDE code.

3. Result and discussion

The reaction between aniline and potassium ferrocyanide produces a precipitate because of the formation of a coordination complex between the ferrocyanide ions and aniline molecules. Aniline has an amino group that can act as a ligand, coordinating with the metal centre of the ferrocyanide ion. The coordination of aniline molecules with the ferrocyanide leads to the formation of a ferrocyanide–aniline complex, which has limited solubility in the solution, resulting in the precipitation of the complex. The complex reacts with nickel chloride, leading to the formation of NFC nanoparticles, where the aniline molecules play a role as a stabilizer, Scheme 1.

X-ray diffraction analysis confirmed the crystalline structure and phase purity of the synthesized NFC, Fig. 2A. The diffraction pattern matched the ICDD reference number 00-057-0049, confirming the formation of NFC, which corresponds to the space group $Fm\bar{3}m$ (225) with lattice parameters $a = b = c =$ 10.0500 Å, $\alpha = \beta = \gamma = 90^{\circ}$, and a unit cell volume of 1015.08 Å^3.[29] The inset figure illustrates the unit cell representation, projected along the *b*-axis. X-ray photoelectron spectroscopy analysis was performed to recognize the electronic states and chemical composition of the synthesized NFC. The survey

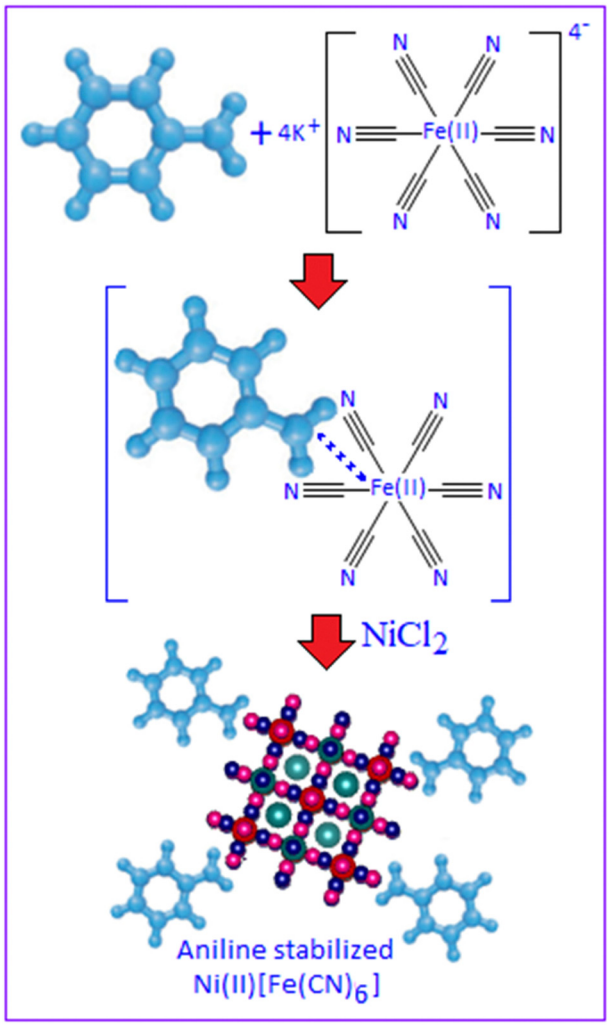

Scheme 1 Formation mechanism of aniline stabilized nickel ferrocyanide nanoparticles.

spectra, Fig. 2B, display the peaks corresponding to Fe, Ni, N and C. The Fe 2p spectrum, Fig. 2C, displays peaks at 708.49 and 721.01 eV, assigned to the Fe $2p_{3/2}$ and Fe $2p_{1/2}$ core levels, characteristic of Fe^{2+} in a ferrocyanide framework.[30] The Ni 2p spectrum, Fig. 2D, exhibited distinct peaks at 856.40 and 874.08 eV, corresponding to the Ni $2p_{3/2}$ and Ni $2p_{1/2}$ core levels, confirming the presence of Ni^{2+}. In addition, the satellite peaks at 863.41 eV and 880.61 eV further supported the Ni^{2+} oxidation state, consistent with the electronic structure of nickel in NFC.[31] The N1 core level spectrum, Fig. 2E, the peaks at 397.6, 398.7 and 402.2 eV signify the existence of C–N in the synthesized material.[32] The two peaks at 284.4 and 285.6 eV in the C 1s core level spectrum, Fig. 2F, correspond to C–C (sp^3) and C–N, respectively.[32] The XPS analysis results confirm the presence of Ni^{2+} and Fe^{2+} oxidation states, validating the successful synthesis of NFC.

Raman spectrum, Fig. 3A, also exhibited the presence of a cyano group (–C≡N) in the range of 1800–2400 cm^{-1}. Two distinct peaks were observed at 2097 and 2135 cm^{-1}, corresponding to the stretching vibrations of the cyano group.[33]

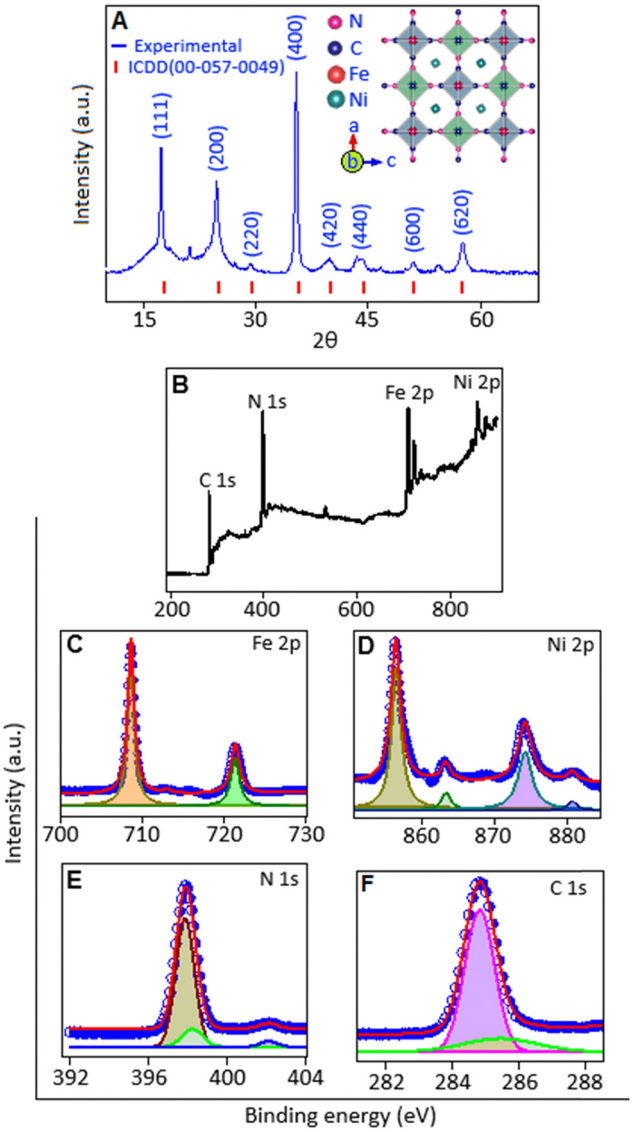

Fig. 2 (A) X-ray diffraction pattern of nickel ferrocyanide with the unit cell diagram (along *b*-axis). (B) XPS survey spectrum of aniline stabilized nickel ferrocyanide nanoparticles. High resolution XPS spectrum of (C) Fe 2p, (D) Ni 2p, (E) N 1s and (F) C 1s.

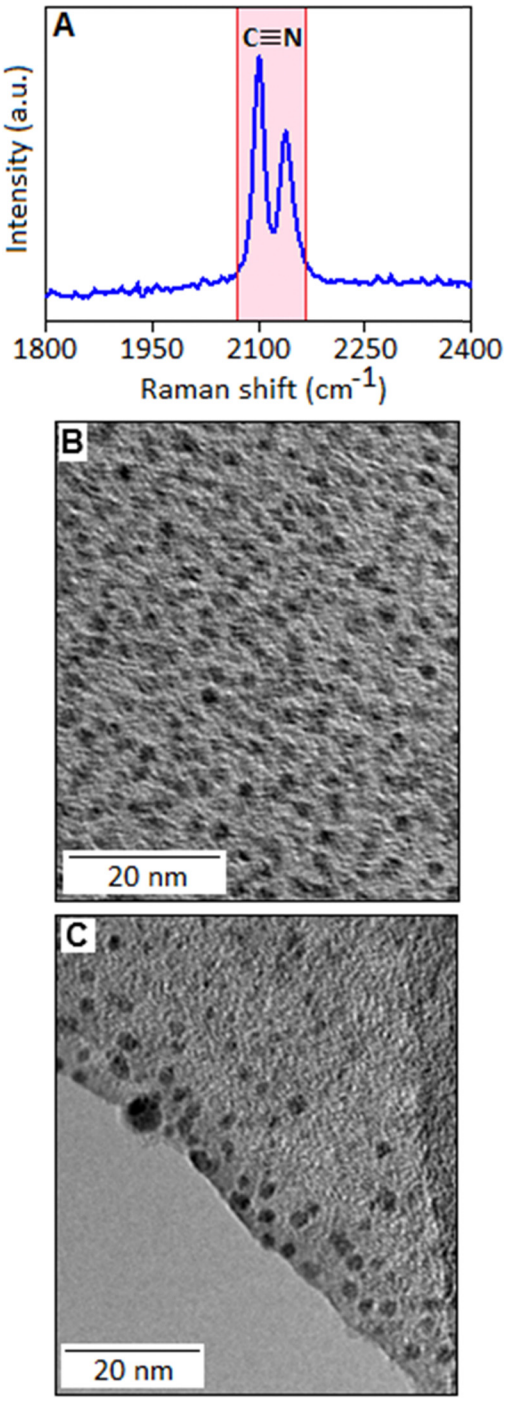

Fig. 3 (A) Raman spectrum exhibited the stretching vibration of the cyano group at 2097 and 2135 cm^{-1}. TEM images (B) and (C) of the aniline stabilized nickel ferrocyanide nanoparticles.

Fig. 3(B and C) presents transmission electron microscopy images of aniline-stabilized NFC at different magnifications. In these images, the contrast observed is primarily due to differences in the electron density of the material, with darker regions corresponding to areas of higher atomic number. The black spots visible in the images represent the individual NFC nanoparticles, which are dispersed throughout the sample. Fig. 3B shows the uniform dispersion of the NFC nanoparticles. Fig. 3C reveals clear and defined boundaries, confirming their size in the range of 3–4 nm.

Fig. 4A, shows the scanning electron microscopy image of the hybrid system. This hybrid material is a combination of organic and inorganic components, with aniline contributing to the organic part and the NFC representing the inorganic portion. The image highlights the surface morphology of the system at a microscopic level. Elemental analysis using the energy dispersive X-ray spectroscopy technique shows the presence of Ni, Fe, C and N in the sample, Fig. 4B. Elemental mapping shows uniform distributions of Ni, Fe, C and N in NFC, Fig. 4(C–F). The elemental mapping also ensures that the aniline and NFC are well-integrated at a microscopic level, without any significant segregation or uneven distribution of the components.

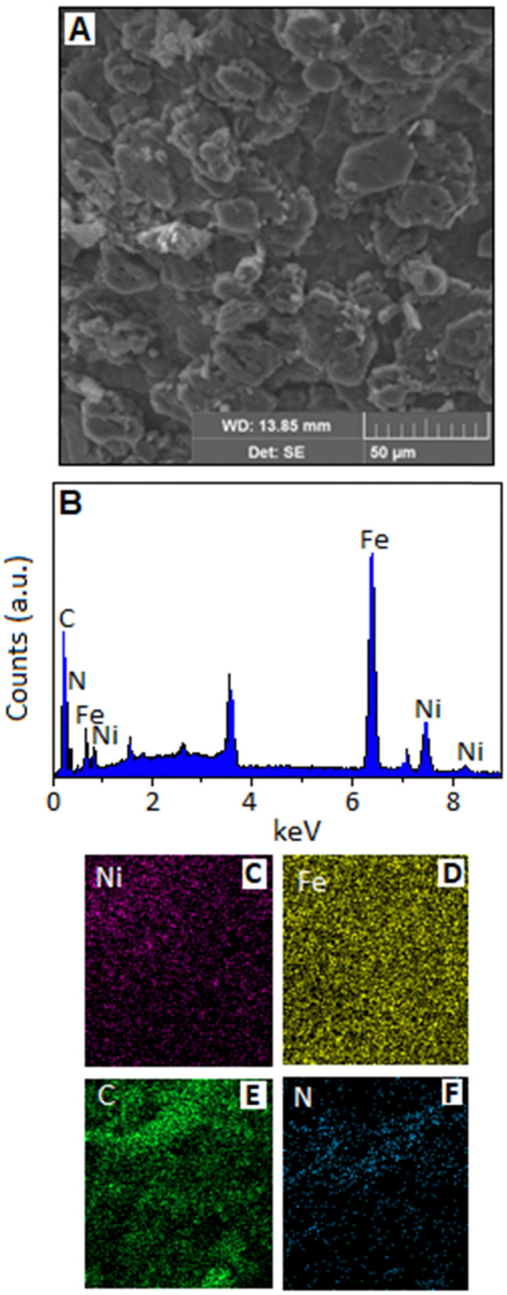

Fig. 4 (A) Scanning electron microscopy image of aniline stabilized nickel ferrocyanide. (B) Energy dispersive X-ray spectrum of nickel ferrocyanide. The elemental mapping of nickel(II) ferrocyanide: (C) nickel, (D) iron, (E) carbon and (F) nitrogen.

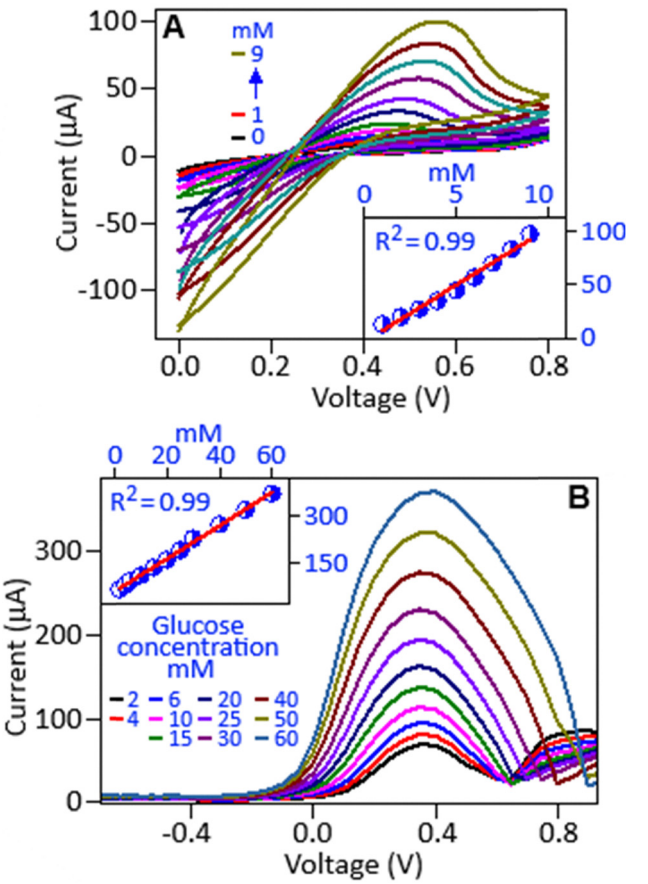

Fig. 5 (A) Cyclic voltammetric response of the nickel ferrocyanide modified working electrode in the presence of glucose, within a concentration range of 0.0–9.0 mM, the inset figure shows the calibration curve. (B) Differential pulse voltammogram of the nickel ferrocyanide modified GCE in the presence of different concentrations of glucose (2.0—60.0 mM), with the calibration curve (inset figure).

3.1. Mechanistic role of the Ni^{3+}/Ni^{2+} redox couple for glucose oxidation

Fig. 5A, main panel, presents the cyclic voltammetric response of the NFC modified GCE electrode in the presence of varying glucose concentrations under a scan rate of 50 mV s^{-1}. As the glucose concentration increases, the peak current also increases within the potential range of 0.5–0.6 V.[34] corresponding to the reversible redox transition of Ni^{2+} to Ni^{3+}. This oxidation peak, observed at 0.56 V, confirms the electrooxidation of Ni^{2+} to Ni^{3+}, which plays a key role in facilitating glucose oxidation, Scheme 2. Fig. 5A, inset, shows a linear relation between the current and the glucose concentration with the limit of detection and sensitivity of 0.97 mM and 1.41 µA mM^{-1} cm^{-2}, respectively. The enzyme-free electrochemical sensor, based on a three-dimensional porous nickel nanostructure, showed a linear range from 0.5 µM to 4 mM with the detection limit and sensitivity values of 0.07 µM and 2.9 mA cm^{-2} mM^{-1}, respectively.[35] It is reported in the literature that nickel oxide nanoparticle modified electrode surface exhibited good linear range from 5 µM to 2.49 mM with the sensitivity and detection limit of 0.310 µA μM^{-1} cm^{-2} and 3.5 µM, respectively.[36] Electrodeposited $NiFeO_x$, supported on nickel foam and carbon cloth, acted as a glucose sensing platform with a sensitivity value of 2320 mA mM^{-1} cm^{-2} and a limit of detection 0.094 mM in the linear range from 0.1–2.1 mM.[37] A nonenzymatic electrochemical glucose sensor based on the hybrid system of nickel nanoparticles and multi-walled carbon nanotubes exhibited linear behavior in the concentration range from 1 µM to 1 mM for the quantification of glucose with a limit of detection of 500 nM.[38]

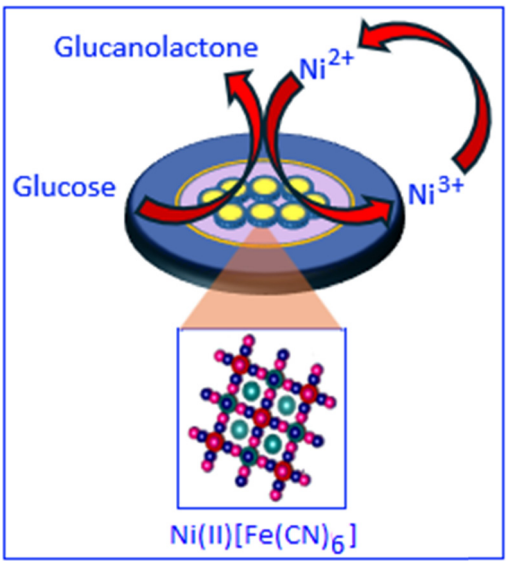

Scheme 2 Glucose oxidation mechanism in the presence of a nickel based catalyst.

Nickel-based compounds are widely regarded as the leading choice for constructing non-enzymatic electrochemical glucose sensors, primarily due to their enhanced catalytic activity, which arises from the redox couple of Ni^{3+}/Ni^{2+} in a NaOH medium. Utilizing nickel compounds as an electrocatalyst for glucose sensing relies on modifying its surface to produce $Ni(OH)_2$, which creates a Ni^{2+} rich surface capable of facilitating the Ni^{3+}/Ni^{2+} redox cycle at a specific potential.[38,39] The Ni^{3+} state in NiOOH oxidizes glucose molecules to gluconolactone, while simultaneously being reduced to the Ni^{2+} state in $Ni(OH)_2$, Scheme 2. It is important to note that we also conducted a cyclic voltammetric study using a ferrocyanide–aniline complex in the presence of glucose (4.0 mM). No characteristic redox peaks were observed, Fig. S1, ESI,† indicating that the Fe^{2+}/Fe^{3+} redox couple does not contribute to the electro-oxidation of glucose.

Differential pulse voltammetry, a highly sensitive electrochemical technique, further validated this redox process, exhibiting a well-defined oxidation peak at 0.4 V, Fig. 5B.[40,41] The oxidation current demonstrated a linear relationship with glucose concentration, Fig. 5B, inset, highlights the electrocatalytic efficiency of the catalyst in glucose oxidation. These findings confirm the critical role of Ni^{2+}/Ni^{3+} redox transitions in non-enzymatic glucose sensing, highlighting nickel-based materials as promising candidates for glucose detection applications with the limit of detection and sensitivity of 1.53 mM and 1.3 μA mM^{-1} cm^{-2}, respectively.

3.2. Extended-gate field-effect transistors (EG-FET) for glucose sensing

The extended-gate field-effect transistor (EG-FET) offers a compact and sensitive approach for electrochemical biosensing, serving as an improved version of the ion-sensitive field-effect transistor (IS-FET).[42] The EG-FET enhances chemical stability and allows integration with different materials by separating the sensing interface from the gate, making it particularly useful for detecting electroactive analytes like glucose, epinephrine and dopamine.[15,42–47]

Compared to the traditional three-electrode system, this setup simplifies the detection process while maintaining high sensitivity and stability. The EG-FET structure consists of a commercial MOSFET, where the metal gate is replaced by a 'working-reference' electrode pair immersed in an electrolyte. The effective gate voltage (V_{eff}) in the EG-FET configuration is given by ($V_{eff} = V_G - V_{ref}$) where V_G is the externally applied gate voltage and V_{ref} is the potential developed between the reference and working electrodes. The potential develops due to the interaction between the working electrode and the electrolyte. As the glucose concentration in the electrolyte increases, it influences the charge distribution at the electrode–electrolyte interface due to glucose oxidation and molecular adsorption.[15,38] These changes alter V_{ref}, thereby modulating V_{eff}, and affecting the n-channel conductivity and output current.

In this study, a NFC-coated ITO electrode was used as the working electrode. The interaction between glucose and the electrode surface induced charge accumulation, altering the voltage between the working and the reference electrodes and modulating the current flow through the transistor channel.[15,46] Fig. 6A shows the output characteristics (current as a function of the drain voltage) at a fixed gate voltage of 2 V, where the addition of glucose caused a gradual decrease in current. This behaviour is attributed to the development of a surface potential between the electrodes, which effectively reduces the applied gate voltage. Fig. 6B presents the transfer characteristics showing the relationship between the drain current and the gate voltage at a fixed source-drain voltage of 0.1 V. As the gate voltage increased, the drain current followed an exponential trend due to channel expansion. Upon glucose addition, a consistent decrease in current was observed across the voltage range. The inset figure shows a linear response of the current value in the presence of various glucose concentrations at 4 V. The estimated detection limit and sensitivity of the EG-FET sensor were 1.12 mM and 0.04 mA mM^{-1} cm^{-2}, respectively. The reusability of the electrode was assessed by employing a single electrode five times to detect 12 mM glucose in the presence of 10 mM NaOH. Fig. 6C shows an increase in the reference voltage after each use, due to charge accumulation from previous measurements. The reproducibility of the electrodes was tested by using 10 individual electrodes to detect 12 mM glucose, resulting in a standard deviation of less than 5%, Fig. 6D.

3.3. Microcontroller based NFC catalyzed glucose sensor

An IoT system was integrated into the experimental setup to provide capabilities for remote data logging and visualization. The Arduino Uno R4 board has an integrated ESP32 chip that can handle Wi-Fi connectivity. The embedded software developed for the microcontroller using the Arduino IDE included routines for interfacing with the sensor to obtain potential measurements. The ESP32 component was configured *via* the Arduino sketch to authenticate and connect to a specified Wi-Fi

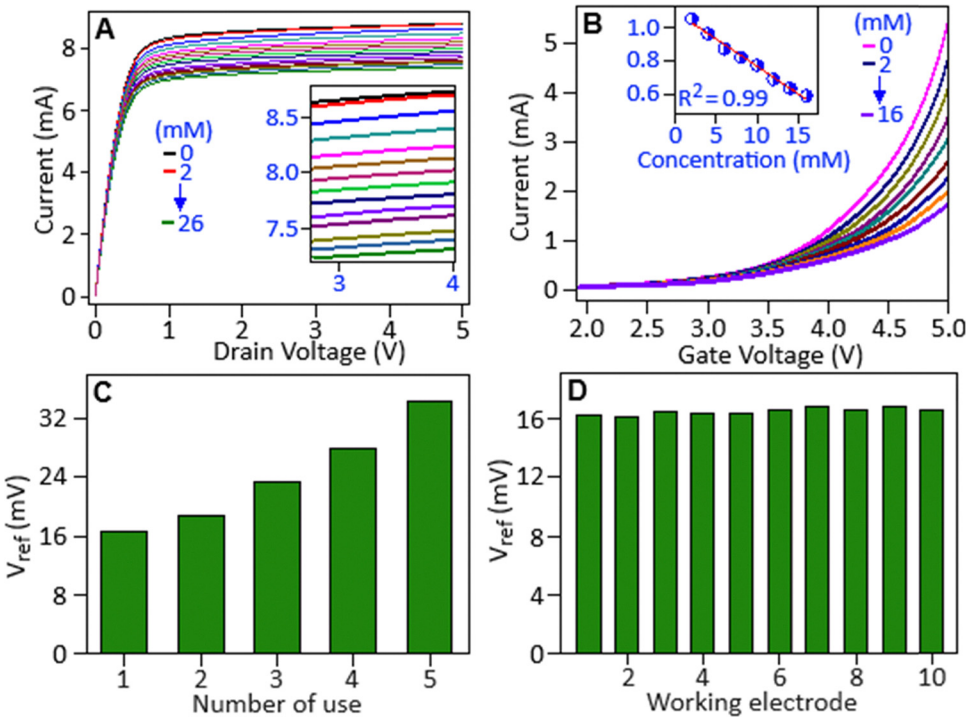

Fig. 6 (A) Output curve (drain voltage as a function of drain current) of the EG-FET in the presence of different glucose concentrations (0.0–26.0 mM) at a constant gate voltage of 2 V. (B) Transfer curve (gate voltage as a function of drain current) at a constant drain voltage of 0.1 V, inset figure represents the calibration curve. (C) Reusability and (D) reproducibility study of the EG-FET based sensor.

network (WPA2 security). Upon successful network connection, the Arduino initiated data transfer to the ThingSpeak cloud platform (MathWorks, USA). Data points were formatted and sent, typically as HTTP GET/POST requests to the ThingSpeak API endpoint associated with a preconfigured channel. ThingSpeak logged the received data, associating each point with a server timestamp, making it accessible globally *via* its web dashboard. This allowed for a near real-time graphical display of the sensor output and long-term data archiving, enabling remote analysis of the sensor over the duration of the experiment.

The EGFET sensor demonstrated a direct relationship between the voltage response and the analyte concentration, enabling real-time glucose monitoring through the measurement of voltage variations, whereas microcontroller based sensors support real-time signal processing and accurate analyte quantification.[44] This integration allows for the accurate detection and measurement of specific chemical or biological substances, with enhanced reliability and performance in analytical applications.[28,48] The response of the sensor was evaluated within a glucose concentration range of 2–12 mM, Fig. 7A, demonstrates a sensitivity of 1.07 mV mM^{-1} with a linearity of 99%, inset (I). The addition of 2 mM glucose induced a measurable voltage shift with a response time of 51 seconds, inset (II).

To evaluate the selectivity of the sensor, an NFC-coated ITO electrode was fabricated and tested in the presence of acetaminophen, lactate, fructose, cholesterol, sucrose and glucose (10 mM). The increment of voltage was observed for each glucose addition, establishing high selectivity of the catalyst, Fig. 7B. To minimize noise and drift, an algorithm was implemented to compute and record the average voltage for 5 seconds. Fig. 7C illustrates the response of the sensor over six hours, maintaining a minimal drift rate of 0.044 mV h^{-1}. Long-term stability was assessed using eight electrodes, stored under ambient conditions. Each week, one electrode was used to detect 10 mM glucose, showing a consistent voltage response, Fig. 7D, which confirmed an extended shelf life and the stability of the NFC based catalyst.

The practical feasibility of the developed microcontroller-based sensor, utilizing nickel ferrocyanide, was assessed by analyzing glucose in commercial artificial saliva. Samples were prepared by adding glucose to the artificial saliva to achieve final concentrations of 2, 4, and 6 mM. Upon introduction into the electrochemical cell of the sensor, the voltage response was measured. The data presented in Table 1 demonstrate the reliability of the sensor under near-physiological conditions, showing minimal relative error, high recovery rates between 99% and 103%, and excellent reproducibility (RSD $< 0.3\%$). These findings, indicating high accuracy and precision, strongly support the potential of this sensor system for practical use in non-invasive glucose monitoring contexts.

The multi-output system, Fig. 1B, of the sensor includes a real-time LCD display, Matplotlib-based data analysis and ThingSpeak cloud integration, providing significant advantages over conventional sensors by enabling remote data monitoring *via* smartphone or web browser, as shown in Fig. S2, ESI.† The compact and portable IoT-enabled design facilitates remote monitoring, making it suitable for telemedicine applications.

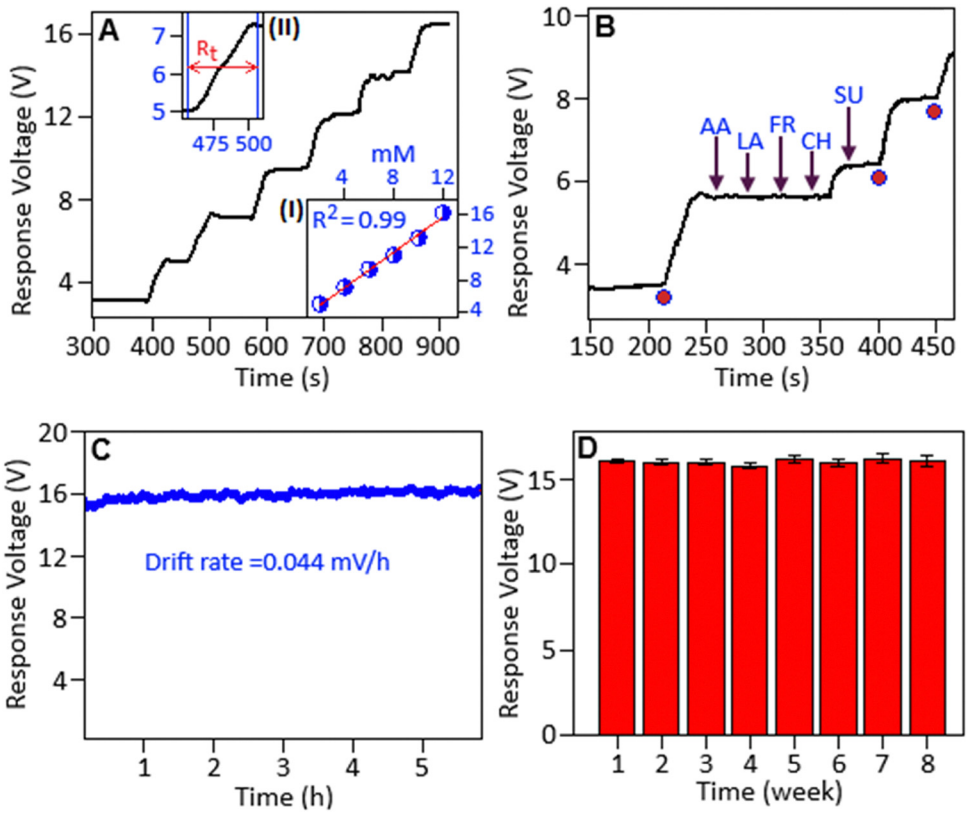

Fig. 7 (A) Response voltage as a function of time with the repeated addition of glucose (2 to 12 mM). Inset figures show the calibration curve (I) and the response time, 52 s, for glucose oxidation (II). (B) Selectivity study of the microcontroller-based sensor for the detection of glucose (Glu), acetaminophen (AA), lactate (LA), fructose (FR), cholesterol (CH) and sucrose (SU). (C) Drift rate and (D) shelf life of the microcontroller based sensor.

Table 1 Glucose detection from an artificial saliva sample using a microcontroller-based IoT sensor

Sample	Added (mM)	Found (mM)	Relative error (%)	RSD (%) (3 measurements)	Recovery (%)
Glucose solution	2	1.98	1.00	0.28	99
	4	4.12	3	0.26	103
	6	5.96	0.67	0.29	99

Table 2 Literature summary of FET and microcontroller-based glucose sensors

Material	Synthesis method	Sensing technique	Sensitivity (mV mM^{-1})	Range (mM)	Linearity	Ref.
ZnO nano array	Sol–gel	FET	0.00039	0.02–0.1	0.967	49
CuO NWs	Etching and heating	FET	3.03	1–12	0.99	46
Nb_2O_5	LPCVD[a]	FET	0.0056	2–7	0.88	50
CuO NPs coated ZnO NRs	Hydrothermal and heating	FET	6.64	1–8	0.98	47
RuO*x*	Sol–gel	FET	6.89	1–8	0.99	51
SnO_2/ITO	RF-sputtering	FET	0.25	2.5–20	0.99	52
Nickel ferrocyanide	Complexation	Micro-controller	1.07	2–12	0.99	(This study)

[a] LPCVD: low pressure chemical vapor deposition.

The NFC-based EG-FET and microcontroller-integrated sensor demonstrate excellent performance in terms of sensitivity, detection range, and linearity, comparable to that of existing reports, listed in Table 2. The advantages include a simple complexation-mediated synthesis, easy electrode fabrication and integration with a low-cost microcontroller, offering a practical and accessible solution for real-time monitoring.

4. Conclusions

In this study, nickel ferrocyanide nanoparticles based on a non-enzymatic glucose sensor were developed where the particles were synthesized through a complexation-mediated route within a size range of 3–4 nm. The structural properties of the synthesized material were thoroughly investigated using

different analytical techniques. The electrochemical performance of the synthesized material was investigated using cyclic voltammetry and differential pulse voltammetry techniques, which demonstrated its catalytic activity for glucose oxidation. This catalytic behavior was primarily driven by the redox transitions between Ni^{2+} and Ni^{3+} ions, which facilitated efficient electron transfer during the oxidation process. The integration of nickel ferrocyanide into an EG-FET configuration provided sensitive glucose detection, with a detection limit and sensitivity of 1.12 mM and 0.04 mA mM^{-1} cm^{-2}, respectively. The performance of the nickel-based catalyst was further explored through a microcontroller-based IoT platform, which enabled real-time monitoring and wireless data transmission. Our findings demonstrate the significant advantages of the non-enzymatic glucose sensor, particularly in terms of stability, reproducibility and operational simplicity. The use of nickel ferrocyanide provides a promising alternative to traditional enzyme-based sensors, mitigating issues such as enzyme degradation and limited operational lifespan.

Data availability

Data will be made available on request.

Conflicts of interest

The authors declare no conflict of interest.

Acknowledgements

This study was supported by the Faculty of Science, University Research Council and the Global Excellence and Stature program 4.0, University of Johannesburg.

References

1 R. Akter, P. Saha, S. Shah, M. Shaikh, M. A. Aziz and A. S. Ahammad, *Chem. – Asian J.*, 2022, **17**, e202200897.
2 T. Kant, K. Shrivas, K. Tapadia, R. Devi, V. Ganesan and M. K. Deb, *New J. Chem.*, 2021, **45**, 8297–8305.
3 V. Vinoth, N. Pugazhenthiran, R. V. Mangalaraja, A. Syed, N. Marraiki, H. Valdés and S. Anandan, *Analyst*, 2020, **145**, 7898–7906.
4 E. Bihar, S. Wustoni, A. M. Pappa, K. N. Salama, D. Baran and S. Inal, *npj Flex. Electron.*, 2018, **2**, 30.
5 M. Filip, M. Vlassa, V. Coman and A. Halmagyi, *Food Chem.*, 2016, **199**, 653–659.
6 Y. Hu, H. Cheng, X. Zhao, J. Wu, F. Muhammad, S. Lin, J. He, L. Zhou, C. Zhang, Y. Deng, P. Wang, Z. Zhou, S. Nie and H. Wei, *ACS Nano*, 2017, **11**, 5558–5566.
7 R. Chen, W. Xu, C. Xiong, X. Zhou, S. Xiong, Z. Nie, L. Mao, Y. Chen and H.-C. Chang, *Anal. Chem.*, 2012, **84**, 465–469.
8 A. Ali, Z. Hussain, M. B. Arain, N. Shah, K. M. Khan, H. Gulab and A. Zada, *Spectrochim. Acta, Part A*, 2016, **153**, 374–378.
9 J. F. Sierra, J. Galban, S. De Marcos and J. R. Castillo, *Anal. Chim. Acta*, 2000, **414**, 33–41.
10 J. Tang, Y. Wang, J. Li, P. Da, J. Geng and G. Zheng, *J. Mater. Chem. A*, 2014, **2**, 6153–6157.
11 M. Mahanthappa, V. Duraisamy, P. Arumugam and S. Senthil Kumar, *ACS Appl. Nano Mater.*, 2022, **5**, 18417–18426.
12 K. Dhara and D. Mahapatra, *J. Mater. Sci.*, 2019, **54**, 12319–12357.
13 M. Rahman, A. Ahammad, J. Jin, S. Ahn and J. Lee, *Sensors*, 2010, **10**, 4855–4886.
14 S. Tee, C. Teng and E. Ye, *Mater. Sci. Eng., C*, 2017, **70**, 1018–1030.
15 K. Shibata and A. Nakamura, *SN Appl. Sci.*, 2022, **4**, 253.
16 H. Begum, M. S. Ahmed and S. Jeon, *RSC Adv.*, 2017, **7**, 3554–3562.
17 N. Myeni, V. Perla, S. Ghosh and K. Mallick, *Mater. Today Commun.*, 2020, **25**, 101291.
18 M. Choudhary, S. Shukla, A. Taher, S. Siwal and K. Mallick, *ACS Sustainable Chem. Eng.*, 2014, **2**, 2852–2858.
19 J. Ramu, S. Ramasundaram, S. Yellappa, L. Gunamalai, T. Kamilya, M. Afzal, A. Anto Jeffery, T. H. Oh, M. Mahanthappa and R. S. Vishwanath, *New J. Chem.*, 2024, **48**, 13814–13824.
20 A. Ensafi, N. Zandi-Atashbar, B. Rezaei, M. Ghiaci, M. E. Chermahini and P. Moshiri, *RSC Adv.*, 2016, **6**, 60926–60932.
21 A. Shamsabadi, H. Tavanai, M. Ranjbar, A. Farnood and M. Bazarganipour, *Mater. Today Commun.*, 2020, **24**, 100963.
22 R. Ahmad, N. Tripathy, M. Ahn, K. Bhat, T. Mahmoudi, Y. Wang, J. Yoo, D. Kwon, H. Yang and Y. Hahn, *Sci. Rep.*, 2017, **7**, 5715.
23 A. Amirsoleimani, H. Siampour, S. Abbasian, G. Rad, A. Moshaii and Z. Zaradshan, *Sens. Bio-Sens. Res.*, 2023, **42**, 100589.
24 R. Reghunath, K. Devi and K. Singh, *Nano-Struct. Nano-Objects*, 2021, **26**, 100750.
25 F. Franceschini and I. Taurino, *Phys. Med.*, 2022, **14**, 100054.
26 M. Choudhary, R. Islam, M. Witcomb and K. Mallick, *Dalton Trans.*, 2014, **43**, 6396–6405.
27 M. Choudhary, S. Siwal, R. Islam, M. Witcomb and K. Mallick, *Chem. Phys. Lett.*, 2014, **608**, 145–151.
28 L. Mgenge, C. Saha, P. Kumari, S. Ghosh, H. Singh and K. Mallick, *Anal. Biochem.*, 2025, **698**, 115726.
29 T. Tatarintseva, O. Mikhailov, N. Naumkina and T. Lygina, *Russ. J. Coord. Chem.*, 2003, **29**, 115.
30 H. Yu, L. Fan, H. Yan, C. Deng, L. Yan, J. Shu and Z. Wang, *Inorg. Chem. Front.*, 2022, **9**, 2001–2010.
31 H. Yu, H. Yan, Y. Xie, C. Deng, X. Zhang, M. Xia, L. Zhang, Z. Wang and J. Shu, *Nano Today*, 2021, **41**, 101327.
32 B. Vishnu, S. Mathi, S. Sriram, B. Karthikeyan and J. Jayabharathi, *Energy Fuels*, 2022, **36**, 1654–1664.
33 Y. Tang, G. Ma, J. Li, M. Liu, B. Xiao and P. Wang, *ACS Appl. Mater. Interfaces*, 2025, **17**, 6560–6567.
34 R. Ouyang, T. Zong, Y. Su, P. Jia, S. Zhou, Y. Yang, K. Feng, H. Chang, Y. Chen, Y. Zhao, F. Xiong and Y. Miao, *J. Solid State Electrochem.*, 2017, **21**, 2887–2898.

35 X. Niu, M. Lan, H. Zhao and C. Chen, *Anal. Chem.*, 2013, **85**, 3561–3569.
36 A. Venkadesh, J. Mathiyarasu, S. Dave and S. Radhakrishnan, *Inorg. Chem. Commun.*, 2021, **131**, 108779.
37 M. Ni, M. Tan, Y. Pan, C. Zhu and H. Du, *J. Mater. Chem. C*, 2022, **10**, 12883–12891.
38 M. Das, T. Chakraborty, C. Y. Lin, R.-M. Lin and C. H. Kao, *Mater. Chem. Phys.*, 2021, **278**, 125652.
39 H. Hu, G. Ma, B. Guo, X. Zhang, R. Xie, H. Liu and H. Huang, *Electrocatalysis*, 2024, **15**, 374–383.
40 N. Karikalan, M. Velmurugan, S. Chen and C. Karuppiah, *ACS Appl. Mater. Interfaces*, 2016, **8**, 22545–22553.
41 M. Rezaeinasab, A. Benvidi, M. D. Tezerjani, S. Jahanbani, A. H. Kianfar and M. Sedighipoor, *Electroanalysis*, 2016, **29**, 423–432.
42 W. Kao, Y. Hung, W. Liao, Y. Chou and C. Lin, *IEEE Trans. Electron Devices*, 2022, **69**, 6304–6309.
43 T. Pan, L. Lin, H. Ding, J. Her and S. Pang, *Talanta*, 2024, **275**, 126178.
44 T. M. Pan, C. Y. Shih and L. A. Lin, *J. Ind. Eng. Chem.*, 2024, **142**, 348–358.
45 C. Saha, S. Kumari, H. Singh and K. Mallick, *Electroanalysis*, 2024, **37**, e202400236.
46 A. K. Mishra, D. K. Jarwal, B. Mukherjee, A. Kumar, S. Ratan and S. Jit, *IEEE Sens. J.*, 2020, **20**, 5039–5047.
47 A. K. Mishra, D. K. Jarwal, B. Mukherjee and S. Jit, *IEEE Trans. NanoBiosci.*, 2022, **21**, 3–9.
48 J. C. Chou, Y. H. Huang, C. H. Lai, Y. H. Nien, P. Y. Kuo, Z. X. Kang and K. T. Lee, *IEEE Trans. Instrum. Meas.*, 2021, **70**, 1–11.
49 D. Jung, R. Ahmad and Y. Hahn, *J. Colloid Interface Sci.*, 2017, **512**, 21–28.
50 C. Kao, H. Chen, L. Kuo, J. Wang, Y. Chen, Y. Chu, C. Chen, C. Lai, S. W. Chang and C. W. Chang, *Sens. Actuators, B*, 2013, **194**, 419–426.
51 K. Singh, B. Lou, J. Her, S. Pang and T. Pan, *Sens. Actuators, B*, 2019, **298**, 126837.
52 C. Liao, J. Chou, T. Sun, S. Hsiung and J. Hsieh, *Sens. Actuators, B*, 2006, **123**, 720–726.

